Mathematical Geology, Vol. 38, No. 5, July 2006 (© 2006)
DOI: 10.1007/s11004-006-9034-z

Semi-Analytic Modelling of Subsidence[1]

Peter A. Fokker[2] and Bogdan Orlic[2]

This paper presents a forward model for subsidence prediction caused by extraction of hydrocarbons. The model uses combinations of analytic solutions to the visco-elastic equations, which approximate the boundary conditions. There are only a few unknown parameters to be estimated, and, consequently, calculations are very fast. The semi-analytic model is applicable to a uniform and layer-cake stratigraphy, with visco-elastic parameters changing per layer, and an arbitrary depletion pattern. By its capabilities to handle a multi-layered visco-elastic subsurface, the semi-analytic model fills the gap between the analytic single-layered elastic models available to date and the more elaborate numerical, e.g. finite element, models.

KEY WORDS: subsidence, reservoir compaction, geomechanics, semi-analytic model, visco-elasticity.

INTRODUCTION

Production of hydrocarbons reduces the reservoir pressure. This pressure change affects the in-situ stress field through poro-elastic coupling. The reservoir may compact, resulting in land subsidence or seabed subsidence. Classical examples are the Wilmington oil field in California (Mayuga and Allen, 1969), the Ekofisk oil field in chalk in the Norwegian sector of the North Sea (Nagel, 1998) and the Groningen gas field in the northern part of the Netherlands (Doornhof, 1992; Houtenbos, 2000).

Rate of compaction at reservoir level and surface subsidence are mutually dependent. Forward modelling can be used if the amount of reservoir compaction is known, or if it can be predicted to an acceptable confidence level, and when existing or future subsidence has to be estimated.

Various authors have studied the subsidence caused by hydrocarbon extraction and proposed methods for subsidence prediction. Geertsma (1973) was the first to apply an analytic, linear forward model, based on the nucleus of strain concept, for a single-layer elastic subsurface. Others have expanded his formulae,

[1]Received 26 August 2004; accepted 8 December 2005; Published online: 2 November 2006.
[2]Netherlands Institute of Applied Geoscience TNO – National Geological Survey, P.O. Box 80015, 3508 TA Utrecht, The Netherlands; e-mail: peter.fokker@tno.nl; bogdan.orlic@tno.nl.

or presented alternatives. Van Opstal (1974) included the effects of a rigid basement. Fares and Li (1988) presented a general image method for a plane-layered elastic medium, which involves infinite series of images. Both analytic solutions are, however, limited to media with two interfaces and therefore to a two-layer model of the subsurface.

A different approach is the use of numerical codes, such as finite elements (Morita and others, 1989; Johnson and others, 1989; Fredrich and others, 1998; Chin and Thomas, 1999). These enable simulation of the full relationship between flow in the porous medium and geomechanics, taking into account complex structural geometry and heterogeneity of the subsurface (Settari and Walters, 2001). In contrast to the analytical models, the numerical models of the subsurface usually demand more time to be constructed and to be computed. There remains, however, a gap between the fast single-layer and two-layer analytical models available to date and the more elaborate finite-element models.

The present paper discusses a multi-layer linear visco-elastic model, of which the elastic part was briefly presented earlier in Fokker (2001). The model presented here is more sophisticated than the available single-layer and two-layer analytical models and requires less computational effort than finite-element calculations. The smaller computational requirements make the method suitable for inversion, i.e. using subsidence data to increase knowledge about compaction at the reservoir level.

A NEW MODEL FOR SUBSIDENCE PREDICTION

The new modelling approach combines elements of analytic and numerical approaches (Fokker, 2001). The method combines a number of analytic functions that satisfy the elasticity equations in such a way that the boundary conditions are approximated. Such an approach makes the method more widely applicable than analytical approaches, while the calculation times are much smaller than for numerical (e.g. finite-element) simulators. It is typically 3 orders of magnitude faster than finite-element calculations and much more flexible in the sense that changes in the elasticity profile are easy to implement.

The method for subsidence prediction has been inspired by a similar concept used by Fitts (1989) for calculation of the pressure field for Darcy flow in a porous medium. Fitts started with the pressure solution of a flowing well in the unlimited three-dimensional space and utilized fields of point sources and sinks distributed around interfaces to fulfil the boundary conditions in a number of selected points. His approach was followed by Fokker and others (2005) to develop a fast model for the productivity prediction of horizontal wells in fractured reservoirs.

The semi-analytic method is similar to boundary-element methods (Crouch and Starfield, 1983). There are, however, a few differences. In the semi-analytic

method singularities are distributed outside the domain, rather than on the boundaries of the domain. Then, the domain is split into multiple regions with different elastic properties. Finally, a least-squares approach is used to approximate the boundary conditions in a number of points rather than to honour them exactly, as it is the case in the conventional boundary element approach. The model can be viewed as belonging to the class of the method of fundamental solutions (MFS). MFS has been reviewed by Fairweather and Karageorghis (1998). The quoted review paper describes the development of MFS over the previous three decades and presents several applications. Our extension is the application to multiple layers of different elastic parameters and to viscoelasticity. Advantages of the approximate solution method of the elasticity equations are that relatively few boundary points and singularities are required, that it does not require elaborate discretization of the boundaries, and that the approximation of the solution and of derivatives can be evaluated directly at any given point. Implementation of the method is relatively easy and computation times are kept low.

The forward model for linear elasticity will be presented first and then extended to linear visco-elasticity.

Elastic Model for Subsidence Above a Centre of Compression

The two equations that are relevant in the theory of linear elasticity are Hooke's law and the equilibrium equation. Hooke's law for linear elasticity, with inclusion of poro-elasticity, reads:

$$\sigma_{ij} = 2G\varepsilon_{ij} + \left[\frac{2G}{1-2\nu}\varepsilon_{kk} - \alpha_{\text{Biot}}\Delta p\right]\delta_{ij} \tag{1}$$

where σ_{ij} is the stress tensor, ε_{ij} is the strain tensor, Δp is the change of pressure, G is the shear modulus, ν is the Poisson's coefficient, α_{Biot} is the Biot's constant and δ_{ij} is the Kronecker delta.

Equation (1) is used further for the difference with the undisturbed state, which is possible due to its linearity. The equilibrium equation reads:

$$\partial_j \sigma_{ij} = 0. \tag{2}$$

The two equations are completed with the boundary and interface conditions. In media with discrete homogeneous elasticity parameters, which are the type of media treated here, the boundary conditions consist of vanishing tractions (σ_{i3}) at

the surface, and continuous tractions and displacements (u_i) at interfaces:

$$\begin{aligned} &\text{surface } (z = 0) : \sigma_{i3} = 0 \\ &\text{interfaces } (z = -d_1 \cdots -d_N) : \begin{cases} \sigma_{i3} = \text{continuous} \\ u_i = \text{continuous} \end{cases} \end{aligned} \tag{3}$$

Solutions to the equations can be conveniently formulated using potential functions such as Galerkin stress functions. Galerkin stress functions, as defined in Mindlin (1936), were used here, including a factor $2G$ in the definition. The factor $2G$ was included for convenient extrapolation to linear visco-elasticity. With a Galerkin vector $\mathbf{F}$, the displacements and the stresses are given by:

$$\begin{aligned} u_i &= 2\,[1-\nu]\,\nabla^2 F_i - \partial_i \partial_k F_k \\ \sigma_{ij} &= 2G\{(\nu\delta_{ij}\nabla^2 - \partial_i\partial_j)\partial_k F_k + [1-\nu]\nabla^2(\partial_i F_j + \partial_j F_i)\}. \end{aligned} \tag{4}$$

In the absence of body forces, the Galerkin vector potential must satisfy the biharmonic equation:

$$\Delta^2 \mathbf{F} = 0. \tag{5}$$

The present study makes use of solutions originating from nuclei of strain. A nucleus of strain refers to a well-defined singularity, for instance a force acting at a single point. A centre of compression, or a centre of compaction, is a nucleus of strain as well, and we use a distribution of these to represent the compacting reservoir. For a nucleus of strain located at $(0, 0, -d)$, the following Galerkin stress functions are associated with a single force directed along the z-axis, a double force (i.e. a single-force dipole), a centre of compression, and a centre-of-compression dipole (also directed along the z-axis); $\mathbf{k}$ is the unit vector in the z-direction; R is the distance to the nucleus, $R = \sqrt{x^2 + y^2 + (z+d)^2}$.

$$\begin{aligned} \mathbf{F}_{\text{single force}} &= \mathbf{k} A R && \text{(a)} \\ \mathbf{F}_{\text{double force}} &= \mathbf{k} B \tfrac{z+d}{R} && \text{(b)} \\ \mathbf{F}_{\text{centre of compression}} &= \mathbf{k} E \log(R + z + d) && \text{(c)} \\ \mathbf{F}_{\text{dipole}} &= \mathbf{k} H \tfrac{1}{R} && \text{(d)} \end{aligned} \tag{6}$$

The constants A, B, E and H are the strengths of the associated nuclei. For a volume dV in which the pressure is reduced by an amount dP, the strength E_0 of the associated centre of compression is given by:

$$E_0 = -\alpha_{\text{Biot}} \frac{1-2\nu}{2G\,(1-\nu)} \frac{dV\,dp}{4\pi} = -c_m \frac{dV\,dp}{4\pi} \tag{7}$$

in which the compaction coefficient c_m has been expressed as a function of the Biot constant α_{Biot}. The compaction coefficient indicates how much a reservoir with a large radius-to-thickness ratio would compact vertically per unit of reservoir thickness and per unit of pressure decrease (it has the dimension of [1/Pa]).

The method employed for solving the elasticity equations with the appropriate boundary conditions starts with the particular solution of the elasticity equations around a centre of compression, embedded in a homogeneous unlimited three-dimensional space, by using its Galerkin stress function (Eq. (6c)). The full solution is applicable in the case of an infinite space with homogeneous properties. The problem at hand, however, involves a subsurface with an unconstrained ground surface and elasticity interfaces at the boundaries between the subsurface layers of different stiffness. The boundary conditions at the ground surface and at the interfaces in a layered subsurface are not honoured by the solution as defined by the centre-of-compression function alone: the fields derived from the stress functions depend on the shear modulus and the Poisson's ratio, G and ν, respectively, and are therefore discontinuous across elasticity interfaces (Figure 1A). The solution originating from the centre of compaction is therefore complemented by other solutions to the elasticity equations to correct for this. The centre of compression in the horizontally layered subsurface, however, does preserve rotational symmetry.

The additional solutions should be chosen in such a way to create additional discontinuities in the tractions and displacements at the layer interfaces and at the ground surface. These solutions should contain free parameters that can be used to fine-tune these discontinuities, so that they can be adjusted to let the resulting complete solution approximate the boundary conditions, viz. continuity of displacements and of tractions at interfaces and zero tractions at the ground surface. Because of the rotational symmetry of the problem, a cylindrical co-ordinate system can be used, and only the r and z-components need to be considered.

The additional solutions are taken as originating from auxiliary nuclei of strain with rotational symmetry along the z-axis (Figure 1B). A number of these nuclei are positioned at different distances from the interface along the z-axis. The field of a nucleus below the interface is applied only above the interface, and vice versa. In this way the singularity is kept outside the domain of application of the elastic field and the solution is a real solution to the elasticity equations in the full application domain. The piecewise application of additional fields induces additional discontinuities in the tractions and displacements. These can be influenced and optimised to meet the boundary conditions, by adjusting the strengths of the nuclei. The set-up of Figure 1 is applicable for a multi-layer subsurface: the fields of the auxiliary nuclei above an interface are applied at all positions below the interface with which it is connected, across the interfaces underneath, and similarly for nuclei below an interface of interest. Clearly, nuclei close to the interface act rather locally, whereas those further away affect a larger volume.

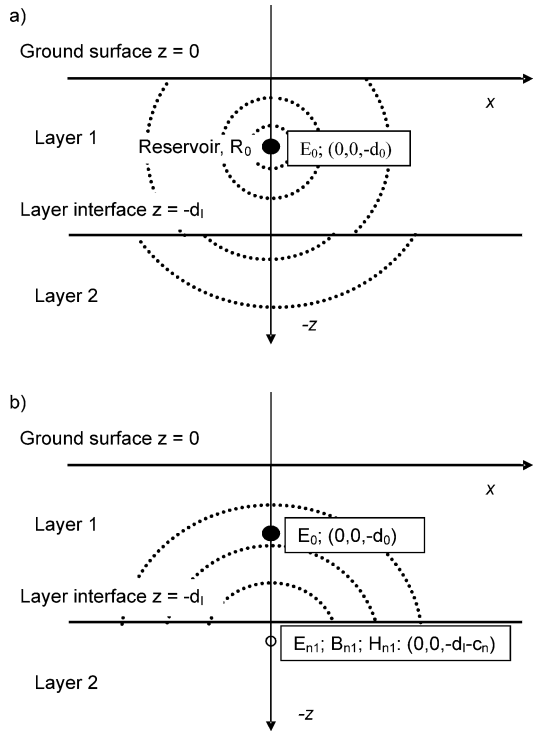

Figure 1. Schematic representation of the conceptual model. (A) The centre of compression of strength E_0, located at (0, 0, $-d_0$), causes stress and strain fields that are discontinuous at the ground surface and at the interfaces between layers of different stiffness. (B) With an auxiliary nucleus of strain E_{n1}, B_{n1}, and H_{n1}, located in layer 2 at (0, 0, $-d_I - c_n$), additional stress and strain fields are generated in layer 1. These fields can be fine-tuned by adjusting the magnitude of the free strength parameters E_{n1}, B_{n1}, and H_{n1}. Solution procedure makes use of several auxiliary nuclei located at different distances from the interface along the z-axis.

To determine the nuclei strengths, first a forward model is constructed with the deviation from the required boundary conditions as outcome. The strengths of the compaction source and of the auxiliary nuclei are input, the latter are unknowns. As this model is linear, a generalized inverse method straightforwardly results in the best estimate for the strengths of the auxiliary nuclei in the least-squares sense. In the least-squares approach, the number of points where the boundary conditions are evaluated exceeds the number of free strength parameters in the solutions of the elasticity equations.

Quality and Robustness of the Method

The quality and robustness of the approximation were tested in order to determine the optimal way of determination of the strengths of the auxiliary sources. Further tests were performed to optimize the number, position and type of the auxiliary nuclei required to use in the model for subsidence prediction.

A first qualitative assessment of the quality of the approximation could be obtained by judging the curves representing the tractions and the displacements at the boundaries and the interfaces. These should be physically sensible: asymptotically approaching zero at infinity; and having the maximum value (or the maximum derivative) at the origin.

A more quantitative judgement of the quality of the approximation was obtained by means of the summed squared deviation from the boundary and interface conditions: the zero tractions at the ground surface, and the zero difference of tractions and displacements at the layer interfaces. Various representations of summed squared deviations were implemented and tested. The most robust scheme was achieved when the strengths of the nuclei were adjusted to minimize the summed squared deviations on a number of equidistant points. For each interface, the equidistant points should extend in the radial direction, starting from the position right on top of the compaction source (E_0), up to 5 to 10 times the vertical distance to it (Figure 2). A value of 7 has been implemented in the code.

The robustness of the approximation was assessed by testing the effect of different elasticity profiles. This was done by judging the quality versus the variation in profile, but also by assessing the variation in the resulting maximum level of subsidence and the variation in the volume of the subsidence bowl for a given centre of compression.

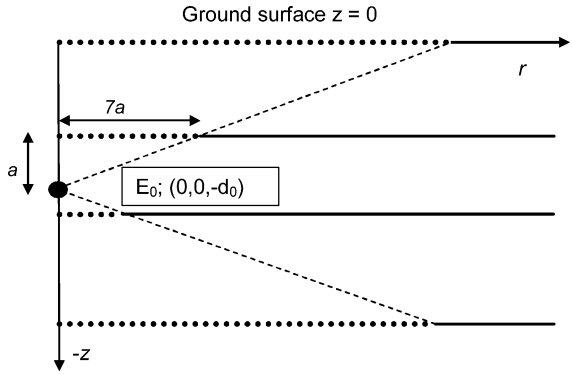

Figure 2. Distribution of the equidistant points at which the interface conditions are evaluated. The distribution extends to 7 times the vertical distance to the compacting source E_0.

The sensitivities to the number of nuclei showed that a reasonable subsidence profile was usually obtained with 6 nuclei for each side of each interface. For elasticity profiles with relatively large contrast in stiffness, i.e. changes in elasticity between adjacent layers larger than a factor of 2, more nuclei were required. 8 to 10 pairs of nuclei around each interface were usually sufficient to obtain accurate results: using 10 pairs instead of 8 often resulted in a fit of better quality, but did not change the resulting subsidence more than 1–2% in terms of depth and 2–5% in terms of volume.

The sensitivities showed that it was absolutely necessary to position the nuclei around the associated interface at distances of the same order of magnitude as the vertical distance of this interface to the original source (i.e. the compacting reservoir). Logarithmically spaced nuclei at distances to the interface of 0.3 to 8 times the distance to the compaction source (E_0) usually gave optimal result. In specific cases this logarithmic pattern of the auxiliary nuclei could be improved, and in some cases it was not possible to achieve an acceptable quality. Such instabilities in the model were usually associated with large contrasts in elastic moduli (larger than a factor 10), large differences in layer thicknesses, or a short distance between the compacting source and one of the interfaces. It is therefore advisable to always check the quality of the approximation before proceeding with the integration exercise.

The sensitivities to the type of the auxiliary nuclei of strain were tested by using different combinations of nuclei types (Eq. (6)). The best results were achieved with combinations of centres of compression, double forces and doublets of centres of compression in the z-direction (Eqs. (6b), (6c), and (6d)). These types of nuclei were also used by Mindlin (1936) to derive the analytical expression for a homogeneous half-space. Including single forces (Eq. (6a)) gave worse results as their fields damp out more slowly than the fields of a centre of compression. Including the dipole (Eq. (6d)) was not strictly necessary but facilitated the same quality of approximation with fewer nuclei. The combination of these three types of nuclei provided sufficient flexibility for our type of problems with circular symmetry around the z-axis. The associated equation for the stresses and the displacements in, e.g., the uppermost layer reads:

$$\begin{aligned}\sigma_{ij} &= \sigma_{ij}(E_0) + \sum_m [\sigma_{ij}(E_m) + \sigma_{ij}(B_m) + \sigma_{ij}(H_m)] \\ &\quad + \sum_{n1} [\sigma_{ij}(E_{n1}) + \sigma_{ij}(B_{n1}) + \sigma_{ij}(H_{n1})] \qquad (8) \\ u_i &= u_i(E_0) + \sum_m [u_i(E_m) + u_i(B_m) + u_i(H_m)] \\ &\quad + \sum_{n1} [u_i(E_{n1}) + u_i(B_{n1}) + u_i(H_{n1})]\end{aligned}$$

where the summations over m are over nuclei above the surface and the summations over $n1$ are over nuclei below the first interface.

Visco-Elastic Model

Most materials show a combination of elastic and viscous behaviour, depending on the time scale. The relaxation time for a visco-elastic material is defined by the ratio between the viscosity (η) and the elastic modulus (E). The actual time scale in relation to this relaxation time determines whether a material behaves in an elastic or viscous way. The most general linear visco-elastic material is described by a linear relationship between a combination of the stress and the stress rate, and the strain and the strain rate tensors. We will assume that the material starts immediately behaving in an elastic manner, and has a long-term viscous reaction. This is known as the Maxwell model, which can be schematized as the series combination of a spring and a dashpot. The tensor form of the constitutive equation of an isotropic Maxwell body is (Ranalli, 1996):

$$\dot{\sigma}_{ij} + \frac{\mu}{\eta}\left(\sigma_{ij} - \tfrac{1}{3}\sigma_{kk}\delta_{ij}\right) = 2\mu\dot{\varepsilon}_{ij} + \lambda\dot{\varepsilon}_{kk}\delta_{ij}. \tag{9}$$

If the Maxwell viscosity η is infinite, the above equation reduces to Hooke's law.

The stress and strain versus time, as described by Eq. (9), are typically slowly varying, non-oscillating functions. In this case, solution with a Laplace transform is the method of choice (Arfken, 1970), in contrast to oscillating functions which are better treated with a Fourier transform. The transform of the time derivative of a function is a linear function of the Laplace transform of the function itself. The Laplace transforms of a function $F(t)$ and of its derivative are given by:

$$\begin{aligned} L\{F(t)\} &= f(s) = \int_0^\infty e^{-st} F(t)\, dt \\ L\{F'(t)\} &= sL\{F(t)\} - F(0) = sf(s) - F(0). \end{aligned} \tag{10}$$

At $t = 0$, the Maxwell body must obey the linear elastic equation:

$$\sigma_{ij}(0) = 2\mu\varepsilon_{ij}(0) + \lambda\varepsilon_{kk}(0)\,\delta_{ij}. \tag{11}$$

With the definition of the Laplace transforms of stress and strain by $\bar{\sigma}(s) = L\{\sigma\}$ and $\bar{\varepsilon}(s) = L\{\varepsilon\}$, the constitutive equation is then transformed to:

$$\bar{\sigma}_{ij} + \frac{\mu}{s\eta}\left(\bar{\sigma}_{ij} - \tfrac{1}{3}\bar{\sigma}_{kk}\delta_{ij}\right) = 2\mu\bar{\varepsilon}_{ij} + \lambda\bar{\varepsilon}_{kk}\delta_{ij} \tag{12}$$

which can be rewritten in the form of the classical linear elastic equations (Eq. (1)) with an equivalent shear modulus and Poisson's ratio, which are now functions of s:

$$\tilde{G}(s) = \frac{\mu}{1 + \mu/s\eta} = \frac{G}{1 + G/s\eta}$$

$$\tilde{\nu}(s) = \frac{\lambda + \frac{1}{3}\mu/s\eta \cdot (2\mu + 3\lambda)}{2\mu + 2\lambda + \frac{2}{3}\mu/s\eta \cdot (2\mu + 3\lambda)} = \frac{\nu + \frac{1}{3}G/s\eta \cdot (1 + \nu)}{1 + \frac{2}{3}G/s\eta \cdot (1 + \nu)}. \quad (13)$$

The boundary conditions also need to be Laplace-transformed. The boundary conditions at the interfaces and the ground surface remain the same, i.e. the continuity of tractions and displacements at the interfaces and zero tractions at the ground surface. The constant value of the nucleus of strain for the centre of compression at the reservoir depth translates into a value of E_0/s in the Laplace domain.

The procedure described above can be used to determine the subsidence profile as a function of s in Laplace space. For a number of suitably chosen values of s, the subsidence profile is determined using the pertinent $\tilde{G}(s)$ and $\tilde{\nu}(s)$, and the transformed nucleus of strength of E_0/s. What needs to be done is the back-transformation to determine the subsidence profile as a function of time.

A number of methods are available to transform function in Laplace space back to the time domain. For oscillatory functions, complex values of the variable s are usually used to obtain satisfactory behaviour. For non-oscillatory functions, a direct inversion of the function in the real Laplace space is often sufficient (Narayanan and Beskos, 1982). We have used a superposition of exponentials as a trial function in the time domain, and we determined the strengths of these contributions such that in the Laplace domain the error in the approximation is minimized (Appendix A). We used the coordinate x as a parameter, because the subsidence profile versus s is fundamentally given in terms of the nuclei strengths and the profile can be calculated numerically at every position as wanted. We consider upgrading the current inversion procedure with the more efficient Gaver-Stehfest method or the Gaver-Whynn-Rho algorithm (Abate and Valkó, 2004; Valkó and Abate, 2004) in our future work.

Integration

The solution obtained by using the method described above yields a subsidence bowl originating from a centre of compression, which is the mathematical representation of an amount of compaction concentrated at a single point. This subsidence bowl is rotationally symmetric. If visco-elasticity is present, the

subsidence bowl is calculated for a number of time-steps. The solution is subsequently used as an influence function or Green function in conjunction with the reservoir data to arrive at the subsidence bowl for the whole reservoir that is compacting. Indicating the influence function for vertical displacement at the surface with $g(r)$, the reservoir height with $H(x, y)$, the pressure depletion with δp and the compaction coefficient with c_m, we have:

$$u_3(x, y) = c_m \int_{\text{reservoir}} H(x', y') \cdot \delta p(x', y') \cdot g\left(\sqrt{(x - x')^2 + (y - y')^2}\right) dx' dy'. \tag{14}$$

For a reservoir with large area compared to its height H, the compaction (which in this case would be purely vertical) would amount to $c_m \cdot H \cdot \delta p$. The integration breaks the rotational symmetry: a reservoir grid of arbitrary outline can be used.

If the reservoir pressures are available from reservoir simulations on discretized models, first the product $\delta V \cdot \delta P$ for the strength of the nucleus is calculated for the centroid of each grid block in the reservoir. Then the integral of Eq. (14) is replaced by a summation over all the active grid blocks in the reservoir:

$$u_3(x, y) = c_m \sum_i \delta V_i \cdot \delta p_i \cdot g\left(\sqrt{(x - x_i)^2 + (y - y_i)^2}\right). \tag{15}$$

The approximation of the influence function of a grid cell by the influence function of a centre of compression in its centre is appropriate as long as the ground surface is far enough away, i.e. the depth is more than 10 times the typical dimension of the grid block. The mismatch is then typically less than 1%. For shallow reservoirs like depleting aquifers, the influence function in Eq. (15) needs to be replaced by a volume integral of the influence function over the grid block.

The new method is applicable to linear theories because it relies on the superposition principle for solutions of the elasticity equations. It can be extended to other linear elastic systems like transverse isotropy or orthotropy, but not to non-linear theories as power-law creep with a coefficient different from unity.

Appendix B provides a detailed description of the algorithm for semi-analytic forward modelling of subsidence.

MODEL VALIDATION

The presented method for calculating the subsidence above a centre of compression has been compared with existing analytical and numerical methods. For simple situations, the method should give results in accordance with solutions that can also be obtained analytically. The approximations introduced at elasticity interfaces call for comparison with a more rigorous technique like finite elements.

The numerical integration over a reservoir grid is straightforward, as demonstrated in an application case study.

Validation with Analytic Tools

We have performed validation exercises with analytical expressions for a single-layer model and a two-layer model, including the limiting case of a two-layer model with a rigid basement. Models with more than two subsurface layers require validation against numerical modelling tools.

The elasticity profile of a two-layer model of the subsurface is used for comparison with analytical techniques (Figure 3). A basement was introduced at a depth of 1,200 m, while the compacting field was located at a depth of 1,000 m, relatively close to the basement. The elastic modulus of the subsurface down to 1,200 m was set to 0.5 GPa and kept unchanged in calculations. The elasticity modulus of the underlying layer, i.e. the basement, was varied.

We performed series of calculations with a two-layer model using the Geertsma model, the model based on the rigid basement theory (Opstal, 1974) and the semi-analytic model. The results of the homogeneous Geertsma model should correspond to the results of the semi-analytic model for the profile without elasticity contrast (i.e., an elastic modulus of 0.5 GPa for the basement), while the rigid basement theory should correspond to the simulation with the rigid basement. The new semi-analytic model was run with 8 nuclei of combined centres of compression, double forces, and centre-of-compression dipoles above the ground surface and around the layer interface, at logarithmically spaced distances of 0.4 to 6 times the distance to the centre of compaction. Three arrays of 8 auxiliary nuclei with each 3 degrees of freedom make the total number of adjusting parameters 72.

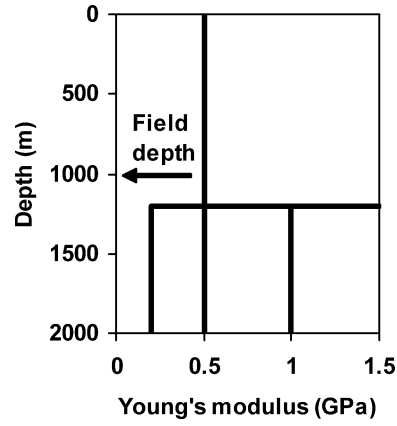

Figure 3. Elasticity profiles of a two-layer elastic subsurface, with varying stiffness of the basement, for testing with analytic methods.

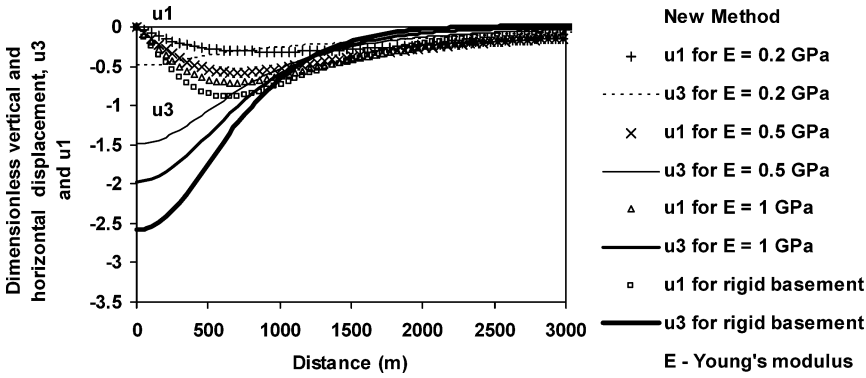

Figure 4. Subsidence predicted by the new semi-analytic method. Elasticity profiles of a two-layer subsurface presented in Figure 3, were used in calculations. The vertical scale is arbitrary since the displacement is linearly dependent on the compacting volume.

A number of values of the basement elasticity have been evaluated with the new method, four of which are presented in Figure 4. The analytical results for the Geertsma model and for the rigid basement model coincide excellently with the results using the new forward model (Figure 5). An average accuracy better than 0.01% has been achieved. This is consistent with the quality judgement that can be made using the form of the curve and the deviation from the boundary conditions, as mentioned earlier. The important observation that can already be made with this straightforward subsurface model is that a distinct effect on the amount of subsidence is already noticed for relatively small stiffness contrasts: when the basement is 20% deeper than the compacting source and its stiffness is

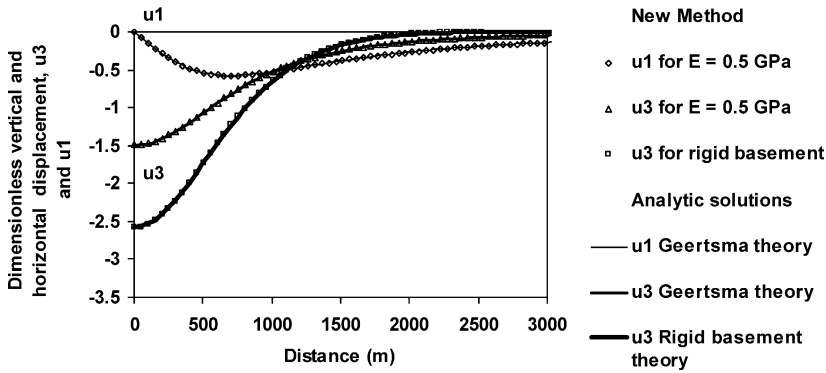

Figure 5. Validation of the new semi-analytic method for subsidence prediction with available analytic methods. The rigid basement theory only provides dimensionless vertical displacement u_3.

only 1.5 times larger than the stiffness of the upper layer, the maximum subsidence increases by 20%. This is entirely due to a narrowing of the subsidence bowl. The increase in maximum subsidence is accompanied by a decrease of the volume of the subsidence bowl. If the basement is less stiff than the overburden, subsidence decreases when compared to a homogeneous subsurface. Actually, the average depth of the reservoir decreases for very small values of the elasticity of the nearby basement.

For validation of the visco-elastic model, we use an analytic solution of the Maxwell model, which is available for a single layer model of the subsurface (Appendix C). The Geertsma method can be applied in the Laplace space and analytically transformed back to the time domain. The resulting vertical displacement at the surface is:

$$u_3(r,t) = -2E_0 \frac{d_0}{\left(r^2 + d_0^2\right)^{3/2}} \left\{ 1 + (1-2\nu) \exp\left[-\frac{2G}{3\eta} (1+\nu)\, t \right] \right\}. \qquad (16)$$

The agreement between the results of the analytic equation and the results of our new method with numeric Laplace back-transformation is clearly excellent (Figure 6). The temporal development of the subsidence bowl can be viewed as a transition of the immediate elastic response with the actual Poisson's ratio to a final situation in which the Poisson's ratio is 0.5—the value associated with a flowing viscous material. A rebound of the subsidence is observed, but the subsidence bowl is not filled in completely because the gravity has not been taken into account.

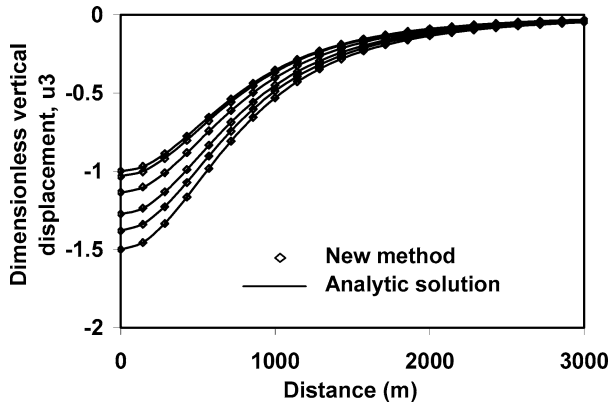

Figure 6. Validation of the Laplace inversion method for calculation of subsidence in a single-layer visco-elastic subsurface with analytic method. Time is increasing, from bottom curve to top, from 0 to 33 times the relaxation time η/G (η—viscosity, G—shear modulus); (steps at 0; 0.33; 0.72, 1.55; 3.33; and 33 times the relaxation time).

Validation with a Numerical Tool

Simulations with a general-purpose finite-element simulator DIANA (1999) were also used to validate the new semi-analytic model. Calculations were carried out on a multi-layer model of the subsurface, with variation in elastic properties in the overburden of the compacting field (Figure 7). An intermediate layer, with deviating elastic properties with regard to the overburden, extends from a depth of 400 to 600 m, and the compacting field is located at a depth of 1,000 m. A rigid basement is present at a depth of 5,000 m. This relatively simple scenario already employs four interfaces, while available analytic approaches are limited to two interfaces. A two-dimensional finite element mesh was extended from the ground surface down to a depth of 5,000 m, with a lateral extension of also 5,000 m.

The nucleus of strain representing the compacting field was created in DIANA by introducing a hollow sphere with a radius of 10 m in which the hydrostatic pressure was negative. The elasticity of the first and the third layer in the overburden was set to 1 GPa; the elasticity of the intermediate layer ranged from 0.1 to 10 GPa. No displacements were allowed at the rigid basement and at the lateral boundary of the model.

The resulting displacements at the ground surface, calculated with the finite element simulator DIANA and with the new method, are in excellent agreement (Figure 8 and Table 1). This demonstrates the validity of the method. In particular, it shows that the approximation of continuity at the interfaces, rather than the rigorous honouring of boundary conditions as in the finite element code, is allowed. For elasticity contrasts larger than a factor 10, the new method may, however, become less accurate.

All validation simulations with DIANA show a discrepancy at the edge of the reservoir. This discrepancy, however, was to be expected due to the

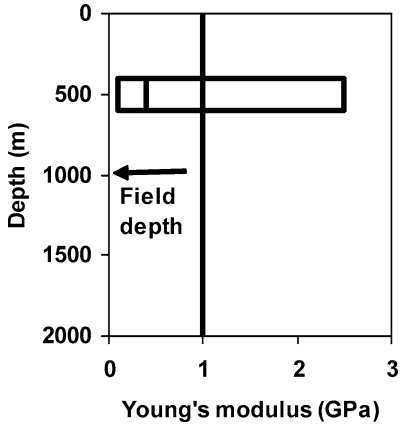

Figure 7. Elasticity profiles of a multi-layer subsurface, with varying stiffness of the overburden, for testing with the finite element simulator DIANA.

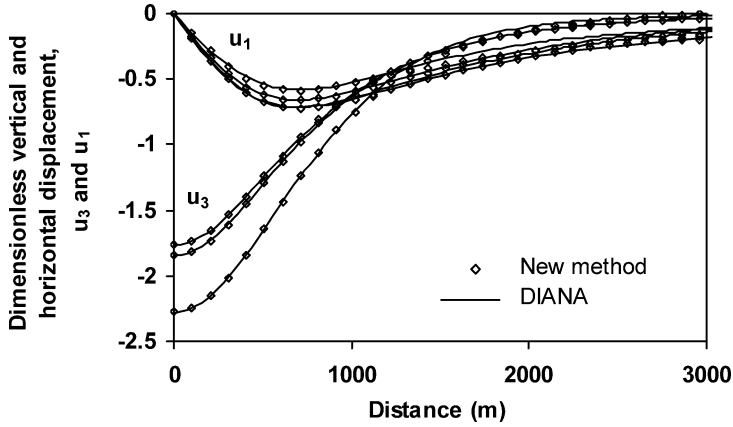

Figure 8. Validation of the new semi-analytic method for subsidence prediction with the finite-element simulator DIANA. Elasticity profiles of a multi-layer subsurface, presented in Figure 7, were used in calculations.

zero-displacement boundary condition introduced in DIANA. Towards the boundary of the model, the semi-analytic approximation can be regarded as more faithful.

For a less stiff intermediate layer (0.1 or 0.4 GPa), the vertical displacement at the ground surface was larger than the reference case with equal moduli, but the horizontal displacement was smaller. This resulted in a wider subsidence bowl. The weak intermediate layer allowed a much larger displacement at the lowest interface, most of which was accommodated by the weak layer. Displacement was distributed laterally throughout this weak layer, resulting in the larger extension of the subsidence bowl at the second interface and at the surface, and in a smaller horizontal displacement at the surface. For stiffer intermediate layers,

Table 1. Maximum Vertical Displacements Resulting from DIANA Finite Element Simulations and from the New Semi-analytic Method

Elasticity modulus, E (GPa)	Maximum subsidence (m)	
	DIANA	New method
0.1	2.279	2.276
0.4	2.042	2.042
1.0	1.845	1.844
2.5	1.763	1.761
10	1.688	1.687

Note. Elasticity profiles of a multi-layer subsurface, presented in Figure 7, were used in calculations.

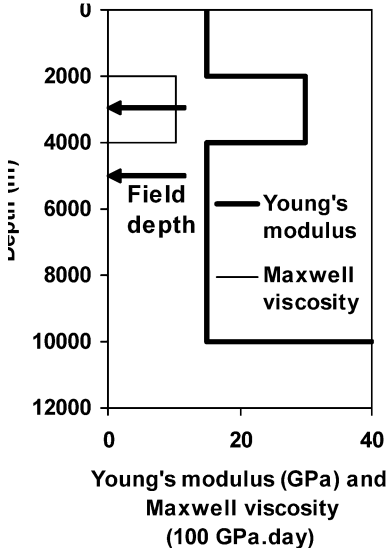

Figure 9. Visco-elasticity profiles of a multi-layer subsurface for testing with the finite element simulator DIANA. The arrows indicate centres of compaction at the depths of 3,000 and 5,000 m.

both horizontal and vertical displacements at the ground surface were smaller than for the reference case. The strong layer resists displacement. Consequently, the difference between vertical displacement at the top and at the bottom is relatively small.

Further validation runs have been performed using DIANA with the constitutive material model of Fokker (1995), who implemented a power-law creep model into the code to simulate salt behaviour. The creep model reduces to a Maxwell model when a unit power-law coefficient is used. We have tested two three-layer scenarios with the DIANA simulator. Both scenarios were run on a multi-layered model of the subsurface, made of two linear elastic layers, one visco-elastic layer in-between the elastic layers and a deep rigid basement (Figure 9).

The first validation is with the centre of compression located in the centre of the visco-elastic layer, at a depth of 3,000 m, and the second with the centre of compression in the lower linear elastic layer, at a depth of 5,000 m. With the centre of compression located in the visco-elastic layer, we calculated subsidence bowls versus time both with DIANA and with the new method. The results show satisfactory agreement (Figure 10). The agreement between the simulations for the centre of compression at a depth of 5,000 m is less satisfactory (Figure 11). This is probably related to the much wider extent of the subsidence bowl and the level of accuracy that the new semi-analytic scheme is able to achieve. The standard deviation becomes larger when the contrast between the (equivalent) shear moduli of the layers becomes larger. This was already indicated in

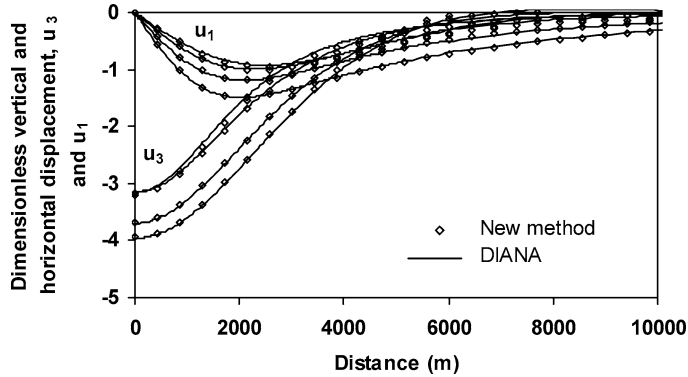

Figure 10. Validation of the new method for subsidence prediction with the finite element simulator DIANA, using the visco-elastic profile presented in Figure 9 and the centre of compression at a depth of 3,000 m. Profiles are shown for zero time, 95 days, 440 days, and 950 days. Vertical displacements are increasing with time, horizontal displacements are decreasing.

the Section on Quality and Robustness above. In the viscoelastic case, large contrasts develop with progressing time, as the viscous character of the salt layer continuously reduces the effective shear modulus to smaller values. However, the trend of a narrowing subsidence bowl in the course of time is faithfully represented.

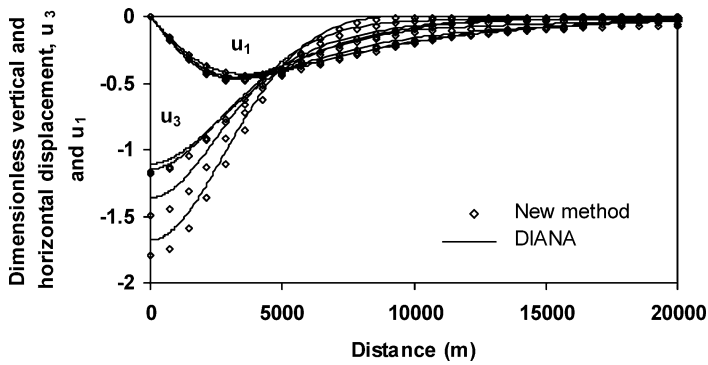

Figure 11. Validation of the new semi-analytic method for subsidence prediction with the finite element simulator DIANA using the visco-elastic profile presented in Figure 9 and the centre of compression at a depth of 5,000. Times are chosen as in Figure 10. The subsidence bowl is deepening and narrowing with increasing time.

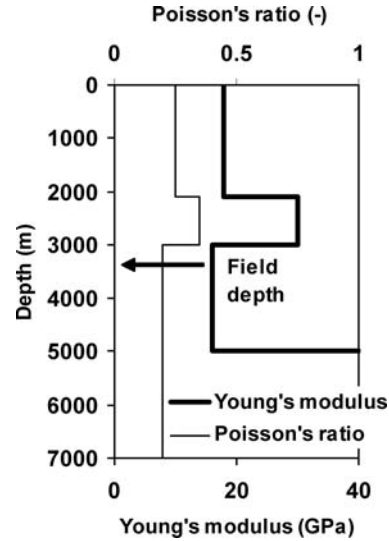

Figure 12. Elasticity profile for the Ameland gas field.

APPLICATION CASE STUDY

The modelling approach developed here was applied to the Ameland gas field in the Northern Netherlands. The Ameland field is produced by NAM (Nederlandse Aardolie Maatschappij B.V.), a joint venture between Shell and Exxon. The field is situated at a depth of 3,350 m, in the Upper Slochteren sandstone, underneath the island Ameland and the wetlands of the Wadden Sea. Having started at an initial pressure of 557 bar, the field will be depleted in 2020 with an abandonment pressure of circa 40 bar.

Over the past twenty years, subsidence in this closely monitored and well-documented field has been modelled using many different techniques (NAM report, 2000). This has resulted in a range of predictions as to what the maximum subsidence will be in the year 2020.

The geomechanical properties of the subsurface in the Ameland region are indicated in Figure 12. The new subsidence prediction model was used in conjunction with this elastic profile to calculate a subsidence bowl for a centre of compression. A two-dimensional grid of compaction coefficient, pressure depletion and net reservoir height was available from reservoir simulation studies by NAM (Figure 13). The profile resulting from the centre of compression was integrated to obtain a subsidence bowl over the whole field, presented in Figure 14. A comparison between Figures 13 and 14 demonstrates that the subsidence bowl is much smoother than the compaction profile that causes it. This is due to a large radius of influence of a centre of compression: at a radial distance equal to

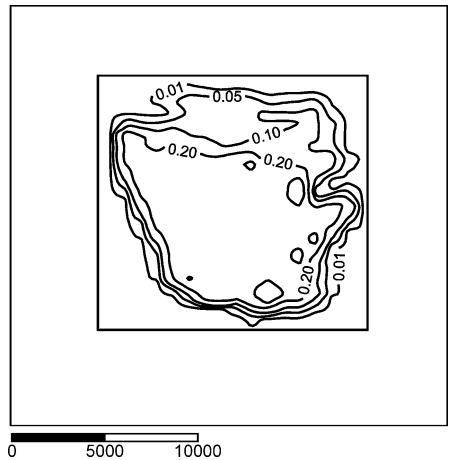

Figure 13. Contour map of the product of (c_m H dP [m]) for the Ameland gas field in the Netherlands. C_m—compaction coefficient, H—net reservoir thickness, dP—depletion pressure. The grid of this product is the compaction source of the subsidence.

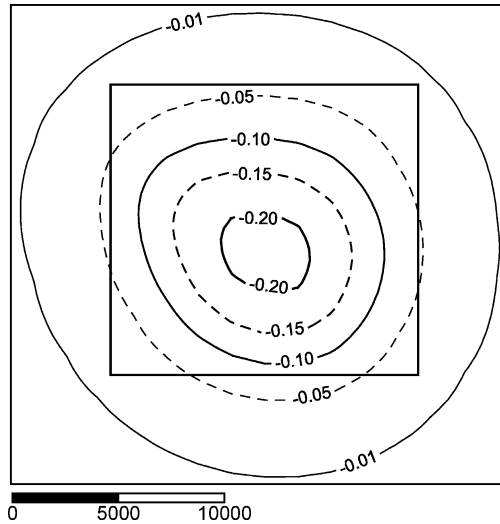

Figure 14. Subsidence bowl above the Ameland field (cm) calculated using the input grid of Figure 13 and the elastic properties of Figure 12. The rectangle indicates the areal extent of the reservoir compaction grid.

the depth of the nucleus, the amount of subsidence is still about one third of the maximum value in the centre of the subsidence bowl.

The maximum amount of subsidence due to the depletion of the Ameland field, expected for 2020, is 0.22 m. This value showed a variation of 20% depending on the elasticity parameters used in calculations. Three different NAM studies had predicted a maximum subsidence of 0.27, 0.19, and 0.28 m. The present results are apparently in line with the earlier NAM predictions.

CONCLUSION

The paper presents a new semi-analytic model for subsidence prediction caused by hydrocarbon extraction. The forward model allows more complexity than current analytical models with respect to the geometry of the model layers and the constitutive behaviour of the geological materials. It is applicable to a uniform and layer-cake stratigraphy, with visco-elastic parameters changing per layer, and an arbitrary depletion pattern. The calculations are very fast and the model is flexible, which makes the semi-analytic approach also suitable for development of a model for inversion of subsidence data.

REFERENCES

Abate, J., and Valkó, P. P., 2004, Multi-precision Laplace transform inversion: Int. J. Num. Methods Eng., no. 60, p. 979–993.

Arfken, G., 1970, Mathematical Methods for Physicist: Academic Press, New York, 815 p.

Chin, L. Y., and Thomas, L. K., 1999, Fully coupled analysis of improved oil recovery by reservoir compaction, SPE paper 56753: Soc. Petrol. Eng. Ann. Tech. Conf. & Exhibition., Houston.

Crouch, S. L., and Starfield, A. M., 1983, Boundary Element Methods in Solid Mechanics: with Applications in Rock Mechanics and Geological Engineering: George Allen & Unwin, London, 322 p.

DIANA, 1999, Program and User's Manual, Release *7.1*: TNO Building and Construction Research.

Doornhof, D., 1992, Surface subsidence in the Netherlands: The Groningen gas field: Geologie en Mijnbouw, no. 71, p. 119–130.

Fairweather, G., and Karageorghis, A., 1998, The method of fundamental solutions for elliptic boundary value problems: Adv. Comp. Math. v. 9, p. 69–95.

Fares, N., and Li, V. C., 1998, General image method in a plane-layered elastostatic medium: J. Appl. Mech., Trans. ASME v. 55, no. 110, p. 781–785.

Fitts, C. R., 1989, Simple analytic functions for modeling three-dimensional flow in layered aquifers: Water Resources Res., no. 25, p. 943–948.

Fokker, P. A., 1995, The Behaviour of Salt and Salt Caverns: unpubl. PhD thesis, Delft University of Technology, The Netherlands, 143 p.

Fokker, P. A., 2001, Semi-analytic subsidence prediction: Proc. Boundary Elements Conference XXIII, p. 117–126.

Fokker, P. A., Verga, F., and Egberts, P. J. P., 2005, New semi-analytic technique to determine horizontal well productivity in fractured reservoirs: Soc. Petrol. Eng. Reservoir Engineering, April issue, p. 123–131.

Fredrich, J. T., Deitrick, G. L., Arguello, J. G., and De Rouffignac, E. P., 1998, Reservoir compaction, surface subsidence, and casing damage: A geomechanics approach to mitigation and reservoir management, Soc. Petrol. Eng. paper 47284: EUROCK'98, v. 1, p. 403–412.

Geertsma, J., 1973, Land subsidence above compacting oil and gas reservoirs: J. Petrol. Technol., p. 734–744.

Houtenbos, A. P. E. M., 2000, The quantification of subsidence due to gas-extraction in The Netherlands: Proc., 6th Int. Symp. Land Subsidence, v. 1, p. 177.

Johnson, J. P., Rhett, D. W., and Siemers, W. T., 1989, Rock mechanics of the Ekofisk reservoir in the evaluation of subsidence: J. Petrol. Technol., July issue, p. 717–722.

Mayuga, M. N., and Allen, D. R., 1969, Subsidence in the Wilmington oil field, Long Beach, Calif., USA, *in* Tison, L. J., ed., Land subsidence, v. 1, no. 88: Internat. Assoc. Sci. Hydrology Publ., p. 6C6–79.

Mindlin, R. D., 1936, Force at a point in the interior of a semi-infinite solids: Physics, no. 7, p. 195–202.

Mindlin, R. D., and Cheng, D. H., 1950, Thermoelastic stress in the semi-infinite solid: J. Appl. Phys., no. 21, p. 931–933.

Morita, N., Whitfill, D. L., Nygaard, O., and Bale, A., 1989, A quick method to determine subsidence, reservoir compaction, and in-situ stress induced by reservoir depletion: J. Petrol. Technol., January issue, p. 71–79.

Nagel, N. B., 1998, Ekofisk field overburden modelling, Soc. Petrol. Eng. Paper 47345: EUROCK'98, v. 2, p. 177–186.

NAM report, 2000, Monitoring of the effects of subsidence on Ameland-East, unpublished (in Dutch).

Narayanan, G. V., and Beskos, D. E., 1982, Numerical operational methods for time-dependent linear problems: Int. J. Num. Methods Eng., no. 18, p. 1829–1854.

Opstal, G. H. C. van, 1974, The effect of base-rock rigidity on subsidence due to reservoir compaction: Proc 3rd Congr. Int. Soc. Rock Mech., v. 2, p. 1102–1111.

Ranalli, G., 1996, Rheology of the Earth: Chapman & Hall, London, 413 p.

Settari, A., and Walters, D. A., 2001, Advances in coupled geomechanical and reservoir modeling with applications to reservoir compaction: Soc. Petrol. Eng. J., September issue, p. 334–342.

Valkó, P. P., and Abate, J., 2004, Comparison of sequence accelerators for the Gaver method of numerical Laplace transform inversion: Comp. Math. Appl., no. 48, p. 629–636.

APPENDIX A: BACK TRANSFORMATION OF THE LAPLACE TRANSFORM

For the back transformation of the Laplace Transform, we use a superposition of exponentials as a trial function in the time domain, and we determine the strengths of these contributions such that in the Laplace domain the error in the approximation is minimized.

The trial function we use in the time domain is:

$$F(x,t) = C_0(x) + \sum_{k=1}^{n_b} C_k(x)\, e^{-b_k t}$$

$$= F(x,0) - \sum_{k=1}^{n_b} C_k(x)\,(1 - e^{-b_k t}) \qquad \text{(A1)}$$

in which it has been assumed that the function $F(x,0)$ is given. $C_k(x)$ are the adjustable coefficients. The key in obtaining an acceptable approximation of $F(x, t)$ is a good set of values for the Laplace variable s and for the parameter b_k. The main time dependent effects occurred for values of the time around the relaxation time of the viscoelastic medium, $\tau = \eta/G$. For zero time, the elastic solution was used; further values for the time were chosen ranging from $\tau/30$ to 30τ. The best coverage of s and b_k to determine profiles for these times were between $30/\tau$ and $1/30\tau$.

The Laplace transform of the function $F(x, t)$ is given by:

$$sf(x,s) = C_0(x) + \sum_{k=1}^{n_b} C_k(x) \frac{1}{1 + b_k/s} = F(x,0) - \sum_{k=1}^{n_b} C_k(x) \frac{b_k}{s + b_k}. \quad \text{(A2)}$$

When for a set of s_i the functions $f(s_i)$ are given, a system of n_s equations can be formulated with n_b unknowns C_k. This system is made over-determined by having more equations than unknowns; i.e. by choosing more values for s_i than for b_k ($n_s > n_b$; n_s is typically 20 and n_b is typically 5).

$$\begin{aligned} \sum_{k=1}^{n_b} A_{ij} C_k(x) &= B_i(x) \\ A_{ik} &= \frac{b_k}{s_i + b_k} \qquad (i = 1..n_s) \\ B_i(x) &= F(x,0) - s_i f(s_i). \end{aligned} \quad \text{(A3)}$$

This system of equations is solved approximately by minimizing its mean square error. This procedure is used to derive a time-dependent value for the subsidence at every position x of the subsidence profile. The error made with profiles typical for the subsidence problem currently studied was less than 0.1%.

APPENDIX B: DESCRIPTION OF THE ALGORITHM FOR SUBSIDENCE PREDICTION FOR A VISCO-ELASTIC SUBSURFACE

The forward model for subsidence prediction proceeds as follows:

- Perform a Laplace transformation on the elasticity equations and choose appropriate values for the Laplace variable, ranging from 0.03 to 30 times G/η, to perform the following actions:
  - Determine the Galerkin stress function belonging to a nucleus of compression at the reservoir depth in an infinite three-dimensional space (Eq. (6c) with $E_0 = 1/s$).

  - Formulate a number of Galerkin functions for nuclei above the ground surface for evaluation of their stress and displacement fields underneath.
  - Formulate a number of Galerkin functions for nuclei around each elasticity interface.
  - Evaluate the boundary conditions at a number of points, yielding a linear set of equations with the strengths of the nuclei as unknowns.
  - Determine the strengths of the auxiliary nuclei by solving the set of equations in a least-squares sense.
  - Evaluate the rotationally symmetric subsidence bowl from the combination of the source nucleus E_0 and the auxiliary nuclei—this is the influence function.
- Perform a numerical Laplace back-transformation on the influence functions to obtain influence functions as a function of time.
- Use the influence function as a Green function and integrate its influence over the compaction field.

APPENDIX C: ANALYTIC SOLUTION OF THE MAXWELL MODEL IN A HOMOGENEOUS SUBSURFACE

The Galerkin stress function given in Equation (4) includes the factor $2G$ in order to relate a centre of compression to a constant amount of fluid or material extracted from the subsurface, even for viscoelastic material. An example for this is a solution mine, where salt has been mined and the cavern has closed up by creep. Without the factor $2G$ the stress would remain constant and the creep would continue perpetually.

The Geertsma solution for subsidence above a centre of compression of strength E_0 in a homogeneous half-space reads:

$$u_3(r) = -4E_0(1-\nu)\frac{d_0}{\left(r^2+d_0^2\right)^{3/2}}. \tag{C1}$$

In the Laplace-transformed space of the visco-elastic medium, the source E_0 is transformed to E_0/s and the Poisson's ratio is replaced by the equivalent Poisson's ratio:

$$\begin{aligned}\bar{u}_3(r,s) &= -\frac{4E_0}{s}(1-\tilde{\nu})\frac{d_0}{\left(r^2+d_0^2\right)^{3/2}} \\ &= -\frac{4E_0}{s}\frac{1+\frac{2}{3}G/s\eta\cdot(1+\nu)-\nu-\frac{1}{3}G/s\eta\cdot(1+\nu)}{\left(1+\frac{2}{3}G/s\eta\cdot(1+\nu)\right)}\frac{d_0}{\left(r^2+d_0^2\right)^{3/2}}\end{aligned}$$

$$= -\frac{4E_0 d_0}{\left(r^2 + d_0^2\right)^{3/2}} \frac{1 - \nu + \frac{1}{3}G/s\eta \cdot (1 + \nu)}{s\left(1 + \frac{2}{3}G/s\eta \cdot (1 + \nu)\right)}$$

$$= -\frac{2E_0 d_0}{\left(r^2 + d_0^2\right)^{3/2}} \left\{ \frac{1}{s} + \frac{1 - 2\nu}{s + \frac{2}{3}G/\eta \cdot (1 + \nu)} \right\} \tag{C2}$$

which can be transformed back analytically:

$$u_3(r, t) = -2E_0 \frac{d_0}{\left(r^2 + d_0^2\right)^{3/2}} \left\{ 1 + (1 - 2\nu) \exp\left[-\frac{2G}{3\eta} (1 + \nu) t \right] \right\}. \tag{C3}$$